INFRARED THERMOGRAPHY FOR COMPLEX FLUID FLOWS

T ASTARITA[1,c]

[1]Dipartimento di Ingegneria Aerospaziale, University of Naples Federico II, Naples, 80125, Italy

[c]Corresponding author: Tel.: +390817685184; Email: astarita@unina.it

KEYWORDS:

Convective heat transfer, flow visualization, IR thermography

ABSTRACT: Infrared Thermography (IRT) is a methodology that allows for: remote detection of thermal energy that is radiated from objects in the infrared band, conversion of such energy into a video signal, and representation of the object surface temperature map. This represents a great potentiality that can be exploited for heat transfer evaluation in a lot of application fields and for many different purposes.

In particular within this contest, measurements performed with infrared (IR) thermography to evaluate wall convective heat fluxes in complex fluid flows are presented. If compared to standard transducers, the infrared camera appears very valuable because it: is non-intrusive, has a high sensitivity (down to 10mK), has a low response time, is fully two-dimensional, so allowing for a better evaluation of errors due to radiation and tangential conduction within the sensor. By correctly choosing the measuring sensor, IR thermography can be exploited to resolve convective heat flux maps with both steady and transient techniques. Finally, the capability of infrared thermography to deal with several simple, or complex, fluid flow configurations is described.

INTRODUCTION

Usually, measuring convective heat fluxes requires both a thermal sensor (with its corresponding thermal model) and some temperature transducers. In the ordinary techniques where temperature is measured by thermocouples, resistance temperature detectors (RTD) or pyrometers, each transducer yields either the heat flux at a single point, or the space-averaged one; hence, in terms of spatial resolution, the sensor itself can be considered as zero-dimensional. This constraint makes experimental measurements particularly troublesome whenever temperature, and/or heat flux, fields exhibit spatial variations.

The Infrared Scanning Radiometer (IRSR) constitutes a true two-dimensional temperature transducer since it allows the performance of accurate measurement of surface temperature maps even in the presence of relatively high spatial temperature variations. When compared to standard techniques, the use of infrared (IR) camera as a temperature transducer in convective heat transfer measurement appears advantageous from several points of view. In fact, since IR camera is fully two-dimensional (up to more than $1M$ pixels), besides producing a whole temperature field, it allows an easier evaluation of errors due to radiation and tangential conduction. Furthermore, it is non-intrusive (e. g., allowing to get rid of conduction through thermocouple or RTD wires), it has high sensitivity (down to $20mK$) and low response time (down to $20\mu s$). As such, IR thermography can be effectively employed to measure convective heat fluxes with both steady and transient techniques.

A first analysis of heat transfer measurements by IR thermography and a review of some of their applications were presented by Carlomagno and de Luca (1989). Three years later, Gartenberg and Roberts (1992) reported an extensive retrospective on aerodynamic research with infrared cameras. More recently, Carlomagno and Cardone (2010) presented a detailed review on infrared thermography for convective heat transfer measurements. The latest review on the basic principles and application of IR thermography to thermo-fluid-dynamics is the book by Astarita and Carlomagno (2012).

In the following two sections first the most commonly used steady and unsteady heat flux sensors will be introduced and then a detailed description of the steady state heated thin foil heat flux will be presented. In the last section some significant applications are reported.

HEAT FLUX SENSORS

The main application of IR thermography in thermo-fluid-dynamics is the measurement of the *convective heat flux* q_c, and/or of the *convective heat transfer coefficient* h between a solid surface and a moving fluid.

The link between q_c and h is the well known Newton's law:

$$q_c = h(T_w - T_r) \tag{1}$$

where T_w is the surface (wall) temperature and T_r is a reference temperature which depends on the fluid flow actual conditions. For example, for iposonic (i.e. small Mach number) external flows the reference temperature practically coincides with the static temperature of the undisturbed fluid. Instead, for high Mach number flows, the correct choice is the *adiabatic wall temperature* (Shapiro 1954 and Schlichting 1979). On the other hand, for iposonic internal flows, the correct choice for the reference temperature T_r is the local bulk temperature in the duct cross section.

In Eq. (1) the heat flux is assumed to be positive if it goes from the surface to the fluid.

Experimental data is usually reported in terms of dimensionless numbers; in particular, both the Nusselt and Stanton numbers are widely used:

$$Nu = \frac{hD}{k_f} \tag{2}$$

$$St = \frac{h}{\rho c_p V} \tag{3}$$

where: D is the hydraulic diameter for internal flows or, in general, a reference length (such as the gap of an annulus, the distance from a leading edge, the boundary layer thickness, etc.); k_f, c_p and ρ are respectively the fluid thermal conductivity coefficient, specific heat at constant pressure and mass density evaluated at film temperature (Bejan 1995); V is a reference velocity.

The Nusselt number is generally used for internal flows while the Stanton number mostly for external flows.

To measure either q_c, or h, a sensor, commonly called *heat flux sensor*, is needed. For IR Thermography applications, the heat-flux sensor generally consists of a slab with a known thermal behaviour, whose surface temperature has to be measured. By properly applying a suitable physical model and the energy conservation equation to the sensor, it is usually possible to find a relationship between the measured temperature and the convective heat flux and/or heat transfer coefficient. When the thermophysical properties of the slab are independent of temperature, the sensor is considered as *ideal*. Frequently, these properties vary only slightly so that it is often possible to assume the heat flux sensor as *ideal*. This hypothesis, together with a constant (in time) T_r, will be generally adopted from now on. The slab surface the flow is going over is called the *front surface* while the opposite one *back surface*.

Three heat flux sensors are generally used with IR thermography:

- *Heated thin foil* sensor. The slab usually consists of a thermally thin metallic foil, or a printed circuit board, steadily and uniformly (in space) heated by Joule effect. Strictly speaking the foil may be heated also in a different way (e.g. by a radiation heat flux to the foil) but then, the heat flux distribution should be precisely known. The convective heat transfer coefficient can be computed by measuring the heat input as well as the foil surface temperature with the IR scanner and by performing a simple energy balance. Due to the foil thermal thinness, the temperature can be measured on either one of the slab surfaces but it is possible to apply this sensor also to not thermally thin foils.
- *Thin film* sensor. A thermally thick slab is used as a sensor and the convective heat transfer coefficient is inferred from the theory of unsteady heat conduction in a semi-infinite solid. The name of the sensor classically derives from to the thin resistance thermometer (thin film), which is bonded to the slab surface and used to measure its temperature. Clearly, the thin film must have negligible heat capacity and thermal resistance as compared to the slab layer affected by the exchanged heat flux. When this sensor is used in combination with an IR scanner, the thin resistance thermometer does not exist but the slab front surface, in contact with the exchanging fluid, must be necessarily viewed by the scanner.
- *Wall calorimeter or thin skin* sensor. The sensor is made of a thermally thin slab (skin) and is used as a pure calorimeter. Being the slab thermally thin, the temperature can be assumed to be constant across its thickness and the

convective heat flux is evaluated from the time rate of the slab temperature change. The use of this sensor with IR thermography is straightforward and either one of the slab surfaces can be viewed by the infrared scanner. Furthermore, as for the heated thin foil, it is easy to make the slab extremely thin because it is unneeded to include, in the sensor, also a temperature detector.

With standard temperature detectors, it is possible to measure the wall temperature only in a relatively small number of discrete points; thus, the additional hypothesis that the sensor should be considered as *one-dimensional* is normally needed. This requirement implies that the heat flux to be measured should be normal to the sensing element surface, i.e. the components of the temperature gradient, which are parallel to the slab plane (tangential), can be neglected. The one-dimensional hypothesis can be dropped when the surface temperature is measured with an IR scanner because of the high data number and spatial resolution of the measurement and this subject will be treated in detail in the following for the heated thin foil sensor.

Recently, heat flux sensors, based on a numerical solution of Fourier's law (typically described by an inverse heat transfer model) and surface temperature measurements, have been developed. The advantage of using such an approach is that it is possible to take into account temperature dependence of thermophysical properties and/or to have slabs with high curvatures.

In the following only the heated thin foil sensor will be discussed; details about the other heat flux sensors can be found in the book by Astarita and Carlomagno (2012).

HEATED THIN FOIL SENSOR

When using IR thermography, the simplest steady state technique, that enables to measure convective heat transfer coefficients, is the heated thin foil sensor. As sketched in Fig. 1*a*, in its classical realization the sensor is made of a thin metallic foil (e.g., an AISI or constantan foil, typically tens of microns thick) steadily and uniformly (in space) heated by Joule effect and thermally insulated at its back surface (right vertical surface in Fig. 1). Since the geometries achievable with a thin metallic foil are quite limited, a possible extension is to use a printed circuit board as a heating element. In this case, often the copper tracks are 5 to 35μm thick and arranged in a Greek fret mode (Cardone et al 1994 and Astarita 1996). Then, it is extremely easy to obtain cylindrical or conical geometries while more complicated forms may be achieved by patching together different "clothes". Ideally, the foil could be heated by any means (e.g. by radiation), even in a non-uniform way, but in such a case, the input heat flux should be precisely known in every point of the sensor. For the sake of simplicity in the following, it will be always supposed that the heating is uniform in space. The heated thin foil practically provides a constant convective heat flux boundary condition.

a) *b*)

Fig. 1 – Sketch of the heated thin foil sensor: *a*) Adiabatic back surface; *b*) Diabatic back surface.

By assuming that the back surface of the sensor is adiabatic, it is easy to perform a simple steady state one-dimensional energy balance per unit area of the sensor:

$$q_j = q_c + q_r \tag{4}$$

where q_j is the imposed input Joule heat flux, q_c is the convective heat flux to fluid and q_r is the radiative heat flux to the flowing fluid ambient.

The radiative heat flux can be computed by using:

$$q_r = \varepsilon_t \sigma \left(T_w^4 - T_a^4 \right) \tag{5}$$

where σ is the Stefan-Boltzmann constant, ε_t is the total hemispherical emissivity coefficient and T_a is the ambient temperature. When standard techniques are used to measure the wall temperature, it is possible to have a very low wall emissivity coefficient (e.g. by gold plating the exchanging surface) so as to neglect the radiative heat flux to ambient. Obviously, this is not the case when measuring temperatures of the front surface by means of IR thermography and, besides, the fluid should be (at least partially) transparent in the used IR band.

From the previous equations and by using Newton's law (1) it is possible to evaluate directly the convective heat transfer coefficient:

$$h = \frac{q_j - \varepsilon_t \sigma \left(T_w^4 - T_a^4 \right)}{T_w - T_r} \tag{6}$$

Under the assumption that the Biot number, $Bi = h_t s/k$ (where s and k are respectively the thickness and thermal conductivity coefficient of the sensor, and h_t includes both convection and radiation) is small as compared to unity, temperature can be considered constant across the foil thickness. Then, it is possible to measure the temperature also of the back surface of the sensor, which, being viewed, obviously becomes diabatic.

If also the back surface is diabatic, (see Fig 1*b*), Eq. (6) must be extended by subtracting from q_j also the total heat flux q_a from the sensor to external ambient, via this surface:

$$h = \frac{q_j - q_a - \varepsilon_t \sigma \left(T_w^4 - T_a^4 \right)}{T_w - T_r} \tag{7}$$

Normally, the heat flux to ambient is the sum of radiative and natural convection heat fluxes. The radiative heat flux can be computed with Eq. (5), while the convective heat flux to external ambient may be evaluated according to the existing situation by using standard correlations tables (e.g. Kays 1993, Perry 1963 and Kakac 1987). However, to carefully evaluate q_a, it is much better to perform some ad hoc tests with the IR scanner, by thermally insulating the front surface, which include the radiative contribute as well (Astarita and Cardone 2000).

It has to be explicitly pointed out that the heat losses q_a and q_r are correction terms and, in order to obtain accurate data, they should be a small fraction of the total Joule heating; otherwise, an error in their evaluation can produce a significant error in the measured h.

The assumption of one-dimensional heat flux sensor is strictly satisfied only if the surface temperature is constant on the sensor surface. However, when using an IR scanner, that is able to measuring surface temperature maps, one is interested in studying complex thermo-fluid-dynamic phenomena where the temperature of the heat flux sensor generally varies in space. Temperature variations on the heat flux sensor surface inevitably cause conductive heat fluxes q_k in a tangential direction. If strong variations of the temperature on the surface of the heat flux sensor are present, the tangential conductive heat flux may constitute an important part of the total heat balance and it cannot be neglected anymore.

For the heated-thin-foil sensor, by retaining the assumption that the slab is thermally thin (i.e. isothermal across its thickness s) and ideal, for isotropic foils, it is possible to evaluate the tangential conduction heat flux per unit sensor area by means of the Fourier law:

$$q_k = -k \nabla_w^2 T_w \tag{8}$$

where ∇_w^2 is the two-dimensional Laplacian operator evaluated in the heat flux sensor plane.

When using an IR scanner, the two-dimensional distribution of the surface temperature is directly measured and, in principle, is straightforward to evaluate the conductive heat flux by numerically approximating the Laplacian in Eq.

(8) with the classical 5 points formula. However, the IR scanner unavoidably generates high frequency random noise that is normally amplified by the numerical derivatives. Therefore, it is indispensable to calculate the Laplacian only after an adequate filtering of the temperature maps. This can be accomplished by a simple convolution with a Gaussian-filtering window. When performing a steady state measurement, to reduce the random noise, it is also helpful to take an average of many temperature maps acquired in a sequence.

When there is an axial symmetry (e.g. an impinging jet or a rotating disk), it is advantageous to perform an azimuthal average of the temperature maps and to calculate the convective heat transfer coefficient only on radial profiles. In particular, in this case the Laplacian of Eq. (8) reduces to the simpler formula:

$$\nabla_w^2 T_w = \frac{\partial^2 T}{\partial r^2} + \frac{1}{r}\frac{\partial T}{\partial r} \tag{9}$$

After having evaluated the tangential conduction heat flux, it is easy to extend the results given by Eq. (7) to the multi-dimensional case. By including this additional term in the energy balance, the convective heat transfer coefficient can be evaluated with:

$$h = \frac{q_j - q_a - \varepsilon_t \sigma\left(T_w^4 - T_a^4\right) - k\nabla_w^2 T_w}{T_w - T_r} \tag{10}$$

As already mentioned, in many applications of the heated-thin-foil sensor, a spatially constant Joule heating can be obtained by using a printed circuit board (Cardone et al 1994 and Astarita 1996). The printed circuit is generally made of a fibreglass support (typically 0.5mm thick) on which extremely thin (5 to 35μm) conductive copper tracks are bonded. The copper tracks are often closely spaced and arranged in a Greek fret mode. Due to the extremely high conductivity coefficient of copper ($k \cong 390 W/mK$), the board exhibits an anisotropic thermal conduction behaviour (along, or across, the tracks) so that, in order to correctly evaluate the tangential conduction term, it is necessary to generalize Eq. (8). This is reported in detail in the paper by Astarita and Cardone (2000) and in Astarita and Carlomagno (2012).

APPLICATIONS

In the following, the heat transfer in three different fluid flow configurations are analyzed by means of infrared thermography by using the steady state *heated-thin-foil* sensor. With this sensor a 180° turn channel with and without V rib turbulators and a rotating disk with and without a centred jet impinging on it are investigated (i.e. an internal flow and an external one).

180° turn channel with and without V ribs

This flow configuration is often encountered inside turbine blades for cooling purposes. Really rib turbulators are often also used in the design of heat exchanger channels in order to enhance the convective heat transfer rate and thus allowing to both reducing the overall exchanger dimensions and to increase efficiency. In 180° turn channels the flow is quite complex due to the various separations and reattachments of the flow and this behaviour it is further enhanced in the presence of rib turbulators.

A two-pass channel of square cross-section $80 \times 80 mm^2$ and $2000 mm$ long before the turn is tested; these dimensions guarantee a hydro-dynamically fully developed flow ahead of the 180° turn. The central partition wall between the two adjacent ducts is $16 mm$ thick and ends with a square tip $80 mm$ distant from the short end wall of the channel. The two side walls of the channels are heated by means of three printed circuit boards and, in case, square rib turbulators ($8 mm$ in side), made of aluminium (to have a high thermal conductance), are glued to them. Ribs have a V shape, with an angle of 45° with respect to the duct axis, have their apex pointing downstream and are placed at a rib-pitch to rib-side ratio P/e of either 10 or 20. Further details about the experimental apparatus can be found in Astarita et al (2002a).

The heat transfer coefficient is calculated by means of Eq. (10) where T_r coincides with the local bulk temperature T_b which is evaluated by measuring the stagnation temperature at the channel entrance and by making a one-dimensional energy balance along the channel. Data are reduced in non-dimensional form in terms of the Nusselt

number normalised by its fully developed counterpart Nu^* (Dittus-Boelter correlation 1930). Both the Nusselt number *Nu* and the Reynolds number *Re* are based on the channel hydraulic diameter.

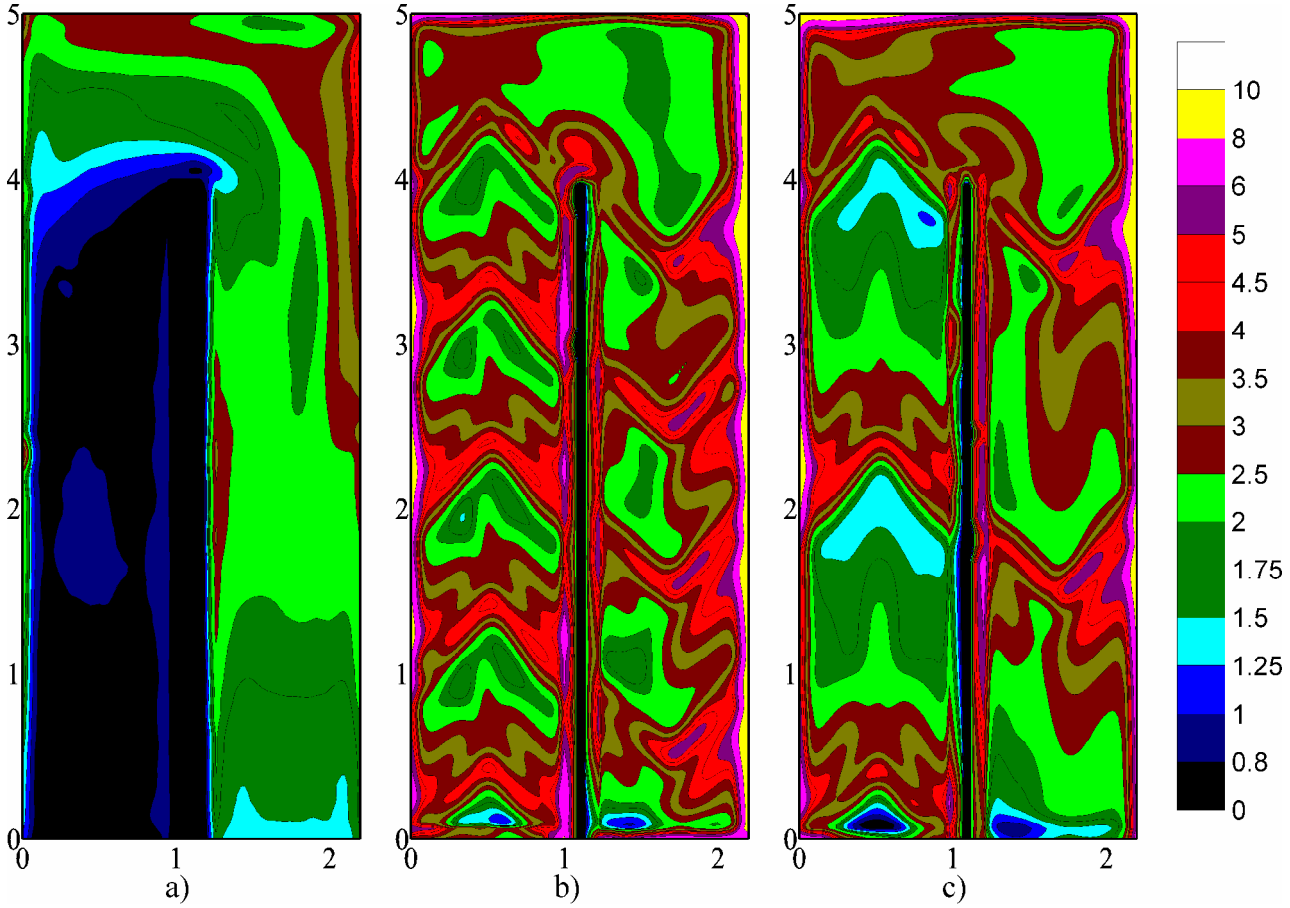

Fig. 2 - Normalised Nusselt number isocontours for *Re*=30,000. *a*) smooth. *b*) *P*/*e*=10. *c*) *P*/*e*=20.

For the smooth channel and *Re* = 30,000, the distribution of the local Nu/Nu^* in the vicinity of the turn, is reported in Fig. 9a. Air enters the channel from the left duct and leaves from the right one. By moving streamwise along the channel, the ratio Nu/Nu^* increases around the turn and downstream of it because of the presence of secondary flows. Three relatively high heat transfer regions may be recognised: the first one is located by the end wall (in front of the partition wall towards the first outer corner) and is caused by the jet coming from the first duct which impinges on this wall; the second one is located at the outer wall downstream of the second corner and is due to the *jet* effect of the flow through the bend; the third one is located at about the half part of the partition wall, downstream of the second inner corner, where the flow rebounding from the outer wall, impinges before exhausting. The second zone attains Nu/Nu^* values much greater than the other two due to the presence of strong secondary flows already found by Arts et al. (1992). Two relatively low heat transfer zones are also observed, one just before the first corner of the outer wall and the other one in the neighbourhood of the tip of the partition wall; these zones constitute evidence for the existence of recirculation patterns.

The overall increase of the convective heat transfer coefficient due to the presence of ribs is clearly evident from Fig. 9b and c where Nu/Nu^*, are shown for the two tested rib-pitch to rib-side ratios *P*/*e*. In all the *Nu* maps ribs are clearly visible due to the higher heat transfer rate that occurs on them. For both dimensionless pitches, the thermal pattern before the turn appears to be repetitive (in a sense, the flow could be considered as thermally *fully developed*). E.g. in Fig. 9b, the shape and levels of the contour lines after the first three ribs of the inlet duct are practically identical. Instead some differences due to some measurements edge effects are found at the duct entrance.

The secondary flows induced by the V-shaped ribs have the form of two pair of counter rotating cells and produce variations in the spanwise Nusselt number distribution both in the inlet and in the outlet channel by decreasing the convective heat transfer coefficient towards the channel axis with respect to that nearby the walls.

Especially in the inlet duct, the reattachment line downstream of the ribs can be identified by the locus of the normalised Nusselt number local maxima when moving in the mean streamwise direction. The reattachment distance, which increases for the higher rib pitch, appears also to increase going from the walls towards the channel axis and this is most likely due to the interaction of the main flow with the secondary one.

In the proximity of the first external corner, it is possible to see a low heat transfer zone, due to a recirculation bubble as already observed for the smooth channel. Just after the last rib and in proximity of the partition wall, the interaction between the secondary flow and the sharp turn produces a high heat transfer zone that tends to shift downstream for increasing pitch.

For both pitches, the overall increase of the turbulence due to the bend induces higher values of the normalised Nusselt number in the outlet duct but the percentage increase is quite lower than what occurring in the smooth channel.

Rotating disk

Rotating systems are quite relevant in several applications and the rotating disk is their simplest configuration. Actually, flywheels, turbine disks blades are attached to, disk brakes and even modern high speed CD-ROMs are all examples of practical applications of this model. Often, the fluid resistance due to rotation is irrelevant but there are a number of cases where the disk thermal behaviour may be important.

The present author with co-workers have applied the IR thermography technique to various rotating disk applications see for example the works by Cardone et al. (1996), Cardone et al. (1997) Astarita et al. (2002b) and Astarita and Cardone (2008). The sketch of the experimental apparatus is shown in Fig. 3; the disk section consists of a 300*mm* (or 450*mm*) in diameter aluminum (or light-alloy steel) cup filled with a 20*mm* thick polyurethane foam, that thermally insulates the face of the disk not exposed to air, on which a circular printed circuit board is glued. Electric power is supplied to the printed circuit by means of a mercury rotating contact. The disk angular speed, which ranges in the interval 100÷4400*rpm*, is precisely monitored by an optical transducer; the angular speed fluctuations are found to be lower than 1%.

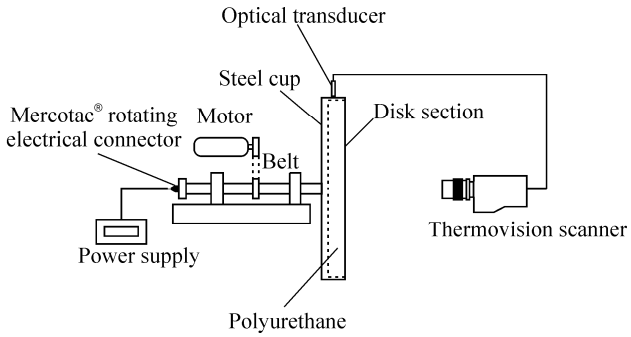

Fig. 3 - Experimental apparatus of Cardone et al (1996).

The importance of the adiabatic wall temperature T_{aw} in relatively high speed flows is illustrated by Cardone et al. 1996. The upper half of Fig. 4 shows the temperature map of the disk rotating at an angular speed ω equal to 4390*rpm* with an imposed Joule heat flux q_j=871W/m^2. The temperature map is an average in time of the real wall temperature and this explain the almost perfect symmetry. The temperature map can be interpreted with an inverse proportionality between temperature and convective heat transfer coefficient. Nevertheless, in the present discussion, the adiabatic wall temperature plays a significant role and some discrepancies can be found.

A relatively small region (≈16% of the disk surface) at the disk centre, where the flow is laminar, is at a constant temperature of about 38.5°*C*. In the central part of the disk, the peripheral disk speed is relatively small and consequently the flow regime is practically iposonic so that the adiabatic wall temperature, shown in the lower half of Fig. 4 and simply obtained with q_j=0 at the some angular speed, practically coincides with the ambient one. The rotating disk laminar solution of Millsaps and Pohlhausen (1952) is:

$$h = ak\sqrt{\frac{\omega}{\nu}} \qquad (11)$$

which does not depend on the radial coordinate r and where a is a constant that for air at ambient temperature (Pr=0.71) turns out to be equal to 0.33.

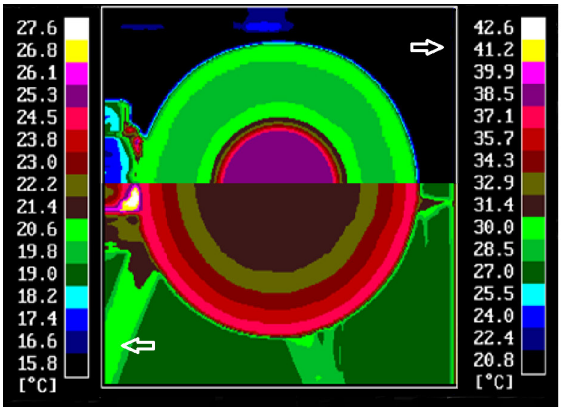

Fig. 4 – Temperature map of the disk rotating at 4390rpm: Upper half T_w (right scale) for q_j=871W/m^2; Lower half T_{aw} (left scale) for q_j=0W/m^2.

Since the convective heat transfer coefficient should be constant over the disk surface, from Eq. (1) it follows that, for a constant heat flux boundary condition and constant T_r, (that in this case is T_{aw}) the wall temperature T_w should be constant. Outside the laminar zone, the wall temperature decreases, first rapidly in the transitional regime and then, more slowly in the turbulent one. Immediately after (besides some edge effects at the disk very periphery) the wall temperature trend is reversed as T_w begins to rise slowly. This behaviour of the wall temperature is unexpected since, according to the turbulent correlation law (e.g. Cardone et al. 1997) the convective heat transfer coefficient should increase for increasing local radius thus, neglecting the adiabatic temperature effects, the temperature should decrease. Actually, the increase of temperature toward the disk limb is easily explained by looking at the adiabatic wall temperature map. In the map, T_{aw} is practically constant (and equal to the ambient temperature) only within the circumference which radius is about 60% of the disk radius; afterwards T_{aw} shows a significant increase (about 3°C near the disk edge). Since for the tested conditions, T_w-T_{aw} is of the same order of magnitude as T_{aw}- T_a, Eq. (1) explains the T_w increase. It has to be explicitly pointed out that, in the case of relatively high Joule heating, the effect of the adiabatic wall temperature would be negligible and a monotonically decreasing wall temperature, towards the disk limb, should be recovered.

Cardone et al. (1997) performed also measurement of the adiabatic wall temperature for a smaller disk (D=150mm) at significantly higher angular speeds (up to 20,600rpm) with the aim to measure the recovery factor:

$$r_f = \frac{T_{aw}-T_a}{\frac{V^2}{2c_p}} = \frac{T_{aw}-T_a}{\frac{\omega^2 r^2}{2c_p}} = \frac{T_{aw}-T_a}{\frac{Re_r\,\omega\nu}{2c_p}} \qquad (12)$$

where in the last term it has been introduced the local Reynolds number $Re_r=\omega r^2/\nu$ based on the local radius r and angular speed ω.

Since the transition from laminar to turbulent regime is found for a fixed value of the local Reynolds number, by looking at Eq. (12) it is clear that in order to increase T_{aw}-T_a in the laminar regime it is necessary to increase the angular speed of the disk and this explains the choice of a smaller disk rotating at a much higher angular speed. The adiabatic wall temperature is plotted in Fig. 5 for various angular speeds. The trend is almost parabolic since the recovery factor varies only slightly by passing from the laminar to the turbulent regime. Data of Fig. 5 can be used to evaluate the recovery factor but, as stated by Astarita (1996), even if the temperature differences are small, the radiative heat flux should not be neglected in the calculation of r_f.

The line scan facility of the Agema 9000 thermographic system has been exploited by Astarita et al. (2002b) to detect the spiral vortices, attached to the surface, which occur in the transitional regime of a simply rotating disk and cause h azimuthal variations. As shown by the blue lines in Fig. 6a the thermographic system scans a horizontal line that is fixed in space. Due to the disk rotation each acquired line is displaced, relative to the disk surface, of an angle

that is function of the rotating speed and of the acquisition frequency. Furthermore, due to the increase in absolute velocity moving towards the disk edge, the scanned line assumes a spiral profile on the disk surface (see lines 1 and 2 in figure). In order to create a thermal map that is stationary with respect to the rotating disk, a numerical reconstruction is performed. Even if, in the line scan mode, the used thermographic system has a maximum acquisition frequency of about 2.5 kHz, which could allow neglecting the spiral deformation of the acquired lines, this effect is taken into account while performing the reconstruction of the thermal images. In order to reduce the noise a large number of radial profiles (about 15,000) are acquired during each test so that each point of the reconstructed image is, really, an average in time of the measured local surface temperature.

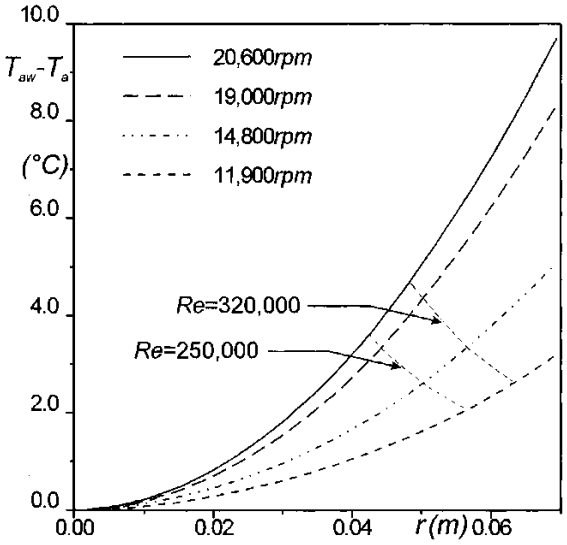

Fig. 5 – Temperature differences on a rotating disk at high angular speed. From Cardone et al. (1997).

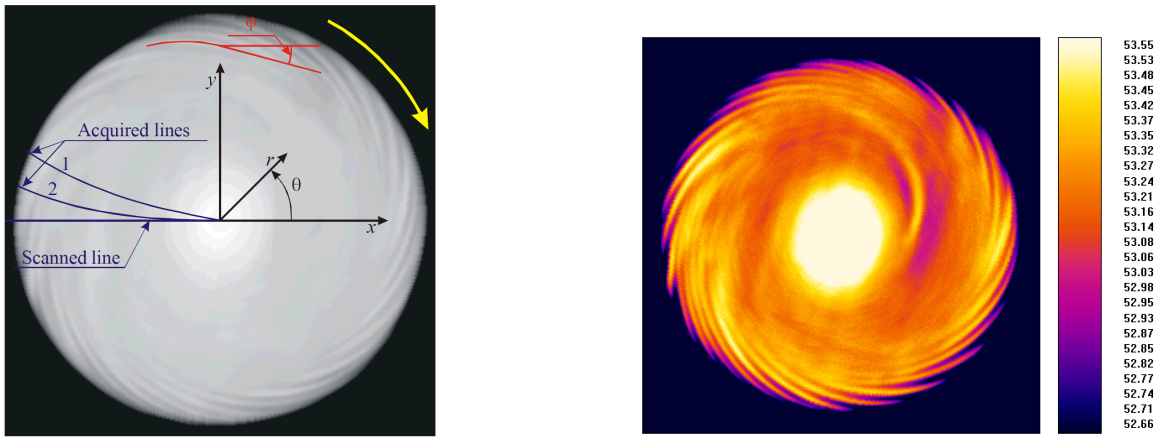

a) b)

Fig. 6 – a) Image reconstruction procedure and b) Reconstruction of spiral vortices on a rotating disk. From Astarita et al. (2002b).

Fig. 6b shows a temperature map of the disk rotating in transitional regime for a total Reynolds number equal to 300,000 and the footprint of the vortices is clearly visible. The disk is rotating in the clockwise direction and its diameter coincides with the side of the external black square. The temperature maps have been used by the authors to measure quantitatively the number of vortices and the spiral vortex angle.

In order to double the camera spatial resolution, the azimuthal reconstruction described before is again used by Astarita and Cardone (2008) to measure the convective heat transfer coefficient on a rotating disk with a small jet impinging at its centre. For each test, about 16,000 lines are used for both the temperature map reconstruction and profile average. They use the same experimental apparatus of Fig. 3 with the addition of a centred jet that is produced

by air that passes through a heat exchanger, a rotameter and finally goes through a nozzle. The heat exchanger ensures a jet bulk temperature practically equal (±0.1°*C*) to the temperature of the ambient air the jet mixes with. Three nozzles with exit diameter *D* from 4 to 8*mm* are in turn used during the tests, the nozzle exit to disk distance *z* varying between 3*D* and 75 *D*. The jet always impinges perpendicularly at the centre of the disk.

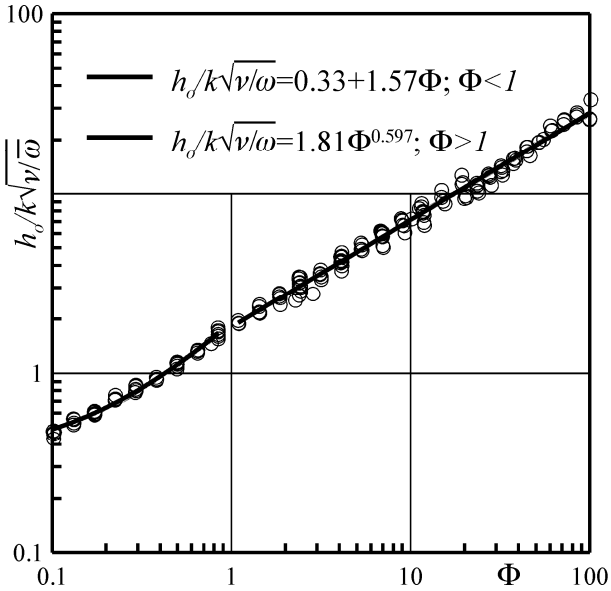

Fig. 7 - Convective heat transfer coefficient at the jet flow stagnation point. From Astarita and Cardone (2008)

In order to reduce the number of governing parameters and because of the lack of theoretical analysis, it is essential to find a rational way to evaluate the relative importance of the jet influence with respect to that due to disk rotation. On the assumption that heat transfer coefficient depends on the flow momentum rate a reasonable dimensionless parameter is the ratio between the two momentum rates (one due to jet, the other one to disk rotation). By assuming a jet width proportional to the distance from the nozzle and laminar flow over the disk, such a parameter can be put in the form:

$$\Phi = \frac{DV}{\nu}\left(\frac{\nu}{\omega z^2}\right)^{\frac{3}{4}} \tag{13}$$

where *V* is the velocity of the fluid at nozzle exit and ν is the kinematic viscosity coefficient.

The nozzle-to-disk distance should be high as compared to *D* so to have jet width proportional to *z*. The convective heat transfer coefficient at the jet stagnation point h_o is examined.

By considering only the disk rotation, the flow is always laminar at the disk centre and h_o can be evaluated from Eq. (11). By considering also the jet effect the h_o departure from the single rotation value should be a function of Φ only. Therefore, the dimensionless quantity $h_o/k\sqrt{\nu/\omega}$ is plotted in Fig. 7 as a function of Φ. In the figure, 160 tests, performed by randomly varying disk angular speed, nozzle diameter, jet initial flow rate and nozzle-to-disk distance, are reported. Since the similitude parameter holds only for high values of the *z*/*D* ratio, even if randomly chosen, *z* always fulfils the condition *z*/*D* > 14.

The experimental data shows a different behaviour for small and large values of Φ. Really, for Φ>1, data appears to be well correlated, in the log-log plane, by a straight line, while the same is not true for smaller values of the parameter, where a linear regression shows a more satisfactory behaviour. Therefore, the equations of the two correlation curves, also shown in Fig. 7 with continuous lines, are:

$$\frac{h_o}{k}\sqrt{\frac{\nu}{\omega}} = 0.33 + 1.57\Phi; \quad \text{for } \Phi < 1 \tag{14}$$

$$\frac{h_o}{k}\sqrt{\frac{\nu}{\omega}} = 1.81\Phi^{0.597}; \quad \text{for } \Phi > 1 \tag{15}$$

The two correlations (14) and (15) are obtained by using 42 and 122 data points and the square correlation factor turns out to be 0.988 and 0.989 respectively and the first one reduces to Eq. (11) for $\Phi = 0$

CONCLUSIONS

The application of infrared thermography as an optical method in heat transfer and fluid flow visualization is analyzed. The heat flux sensors, which are normally used for the measurements of convective heat transfer coefficients, and the application of the infrared scanning radiometer as a temperature measuring device are critically reviewed. In particular the corrections of the errors associated with tangential conduction along the sensor are investigated for the heated-thin-foil sensor.

The heated-thin-foil heat flux sensor coupled with measurement of surface temperature by IR thermography is used to measure the convective heat transfer coefficient on two flowfields: a 180° turn channel with and without rib turbulators and a rotating disk with and without a centered jet impinging on it.

In the inlet zone, ribbed channels show spanwise variations of the heat transfer maps because of the presence of secondary flows. For both tested rib pitches the overall increase of turbulence due to the bend induces higher values of the normalized Nusselt number but, in the outlet duct the percentage increase is lower than that relative to a smooth channel because of the rib already induced turbulence.

For a simple rotating disk experimental data is correlated in terms of Nusselt and Reynolds numbers, both based on the local radius and shows to be in accordance with theoretical predictions. The spiral vortices that arise in the transitional regime are also investigated. To correlate the influence of a small centred jet perpendicularly impinging on the disk on the convective heat transfer coefficient, it has been assumed that the convective heat transfer coefficient is proportional to the momentum flux. Therefore, a similitude parameter, which is proportional to the ratio between the two momentum fluxes due respectively to the jet and to the rotation of the disk, has been proposed. A satisfactory correlation for the convective heat transfer coefficient at the disk centre has been introduced.

REFERENCES

1. Arts T, Lambert de Rouvroit M, Rau G and Acton P Aero-thermal investigation of the flow developing in a 180 degree turn channel, Proc. Int. Symp. on Heat Transfer in Turbomachinery, Athens, 1992.
2. Astarita T and Cardone G, Convective heat transfer on a rotating disk with a centred impinging round jet. Int. J. Heat Mass Transf., Vol. 51, pp. 1562-1572, 2008.
3. Astarita T and Cardone G, Thermofluidynamic analysis of the flow in a sharp 180° turn channel. Exp. Therm. Fluid Sci., Vol. 20, pp. 188-200, 2000.
4. Astarita T and Carlomagno G M, Infrared thermography for thermo-fluid-dynamics, Springer, Berlin, 2012
5. Astarita T, Alcuni aspetti di scambio termico nelle turbine a gas. Phd thesis, Universita di Napoli, 1996.
6. Astarita T, Cardone G and Carlomagno G M, Convective heat transfer in ribbed channels with a 180° turn, Experiment in Fluids, Vol. 33, pp. 90-100, 2002a.
7. Astarita T, Cardone G and Carlomagno GM, Spiral vortices detection on a rotating disk. In Proc. 23rd Cong Int. Council Aeronautical Sciences, paper n. ICAS2002-3.6.4, 2002b.
8. Bejan A, Convective Heat Transfer. Wiley, New York, 1995.
9. Cardone G, Astarita T and Carlomagno GM, Heat transfer measurements on a rotating disk in still air. In Proc. Flucome'94, Vol. 2, pp. 775-780, 1994.
10. Cardone G, Astarita T and Carlomagno GM, Heat transfer measurements on a rotating disk. Int. J. Rot. Mach., Vol. 3, pp. 1-9, 1997.
11. Cardone G, Astarita T and Carlomagno GM, Infrared heat transfer measurements on a rotating disk. Optical Diagnostics in Engineering, Vol. 1, pp. 1-7. 1996.
12. Carlomagno GM and Cardone G, Infrared thermography for convective heat transfer measurements. Exp. Fluids, Vol. 49, pp. 1187-1218, 2010.

13. Carlomagno GM and de Luca L, Infrared thermography in heat transfer. In Handbook of Flow Visualization, WJ Yang, editor, Hemisphere, Washington, DC, Vol. 32, pp. 531-553, 1989.
14. Dittus P W and Boelter L M K, Heat Transfer in Automobile Radiators of the Tubular Type, Univ. Calif. Pub. Eng., Vol. 2, N. 13, pp. 443–461, 1930 (reprinted in Int. J. Comm. Heat and Mass Transfer, 12, 3-22, 1985.).
15. Gartenberg E and Roberts A S, 25 years of aerodynamic research with infrared imaging. J. Aircr., Vol. 29, pp. 161-171, 1992.
16. Kakac S, Shah R K and Aung W, Handbook of Single Phase Flow Convective Heat Transfer, Wiley, New York, 1987.
17. Kays W M and Crawford M E, Convective Heat and Mass Transfer, Mc Graw–Hill, 1993.
18. Millsaps K and Pohlhausen K, Heat transfer by laminar flow from a rotating plate. J. Aero. Sci., Vol. 19, pp. 120-126, 1952.
19. Perry J H, Chemical Engineers' Handbook, Mc Graw-Hill, 1963.
20. Schlichting H, Boundary-layer theory. McGraw-Hill, New York, 1979.
21. Shapiro, AH, The Dynamics and Thermodynamics of Compressible Fluid Flow, Vol. I and II, Ronald Press, New York, 1954.